Model for how retrograde actin flow regulates adhesion traction stresses

2010 J. Phys.: Condens. Matter 22 194113

(http://iopscience.iop.org/0953-8984/22/19/194113)

J. Phys.: Condens. Matter **22** (2010) 194113 (11pp) doi:10.1088/0953-8984/22/19/194113

Model for how retrograde actin flow regulates adhesion traction stresses

Ying Li[1], Prabhakar Bhimalapuram[2,3] and Aaron R Dinner[2,4]

[1] Department of Physics, James Franck Institute, and Institute for Biophysical Dynamics, The University of Chicago, Chicago, IL, USA
[2] Department of Chemistry, James Franck Institute, and Institute for Biophysical Dynamics, The University of Chicago, Chicago, IL, USA

E-mail: dinner@uchicago.edu

Received 21 October 2009, in final form 11 March 2010
Published 26 April 2010
Online at stacks.iop.org/JPhysCM/22/194113

Abstract
Cells from animals adhere to and exert mechanical forces on their surroundings. Cells must control these forces for many biological processes, and dysfunction can lead to pathologies. How the actions of molecules within a cell are coordinated to regulate the adhesive interaction with the extracellular matrix remains poorly understood. It has been observed that cytoplasmic proteins that link integrin cell-surface receptors with the actin cytoskeleton flow with varying rates from the leading edge toward the center of a cell. Here, we explore theoretically how measurable subcellular traction stresses depend on the local speed of retrograde actin flow. In the model, forces result from the stretching of molecular complexes in response to the drag from the flow; because these complexes break with extension-dependent kinetics, the flow results in a decrease in their number when sufficiently large. Competition between these two effects naturally gives rise to a clutch-like behavior and a nonmonotonic trend in the measured stresses, consistent with recent data for epithelial cells. We use this basic framework to evaluate slip and catch bond mechanisms for integrins; better fits of experimental data are obtained with a catch bond representation. Extension of the model to one comprising multiple molecular interfaces shifts the peak stress to higher speeds. Connections to other models and cell movement are discussed.

(Some figures in this article are in colour only in the electronic version)

1. Introduction

In animals, adhesion of cells to the extracellular matrix (ECM) is important for their migration as well as the formation and maintenance of structures in tissues. The cytoskeletal network of actin filaments and associated proteins inside each cell is connected to the ECM through micron-scale mechanosensitive assemblies of proteins known as focal adhesions (FAs) [1–3]. Although the specific composition of FAs, which contain 50 or more different proteins, remains elusive, binding to the ECM is mediated by members of the integrin family of integral membrane proteins. Because various kinases and actin binding proteins are also found in FAs, these assemblies are thought to act as hubs for integrating mechanical forces and signaling cascades to enable cells to sense and respond to their physical environment. However, many proteins within FAs are likely to perform context-specific structural and biochemical roles. It is thus difficult to parse the mechanisms that regulate the dynamics of these assemblies by traditional approaches.

To delineate the relation between force and FA dynamics, several groups have sought to relate quantitative force measurements to observations in microscopy experiments. Initially, forces were estimated by the degree to which cells wrinkled an elastic substrate [4]. Improved spatial and temporal resolution was obtained by modifying the substrate such that it no longer wrinkled, and forces were instead measured by tracking embedded fiducial markers [5–7]. Alternative approaches that measure deformation of a cantilever [8] or an elastomeric post [9, 10] significantly

[3] Present address: Center for Computational Natural Sciences and Bioinformatics, International Institute of Information Technology, Gachibowli, Hyderabad 500 032, India.
[4] Address for correspondence: Gordon Center for Integrative Science, 929 East 57th Street, Chicago, IL 60637, USA.

simplify the back calculation of forces from images. Internally or externally derived forces up to a few nanonewtons per adhesion appear to promote the growth of adhesions in their direction [9–11]. FA size and post-forces were observed to be correlated in fibroblasts [9, 10]. Consistent with these observations, FA size depends on the local stiffness of the ECM [12, 13]; inhibition of myosin II, and thus contractility of the actin cytoskeletal network, reduces FAs (see [3] and references therein). Models that account for force-induced anisotropic growth have been developed and elaborated [14–19]. Essentially, tension-induced variations in protein density shift the balance between exothermic adsorption of new proteins and the energetic cost of elastic deformation to different extents at the front and rear of a FA.

Nevertheless, an outstanding question is how the flow of proteins within cells impacts FAs and the forces they mediate. The flow of actin is directed from the leading edge to the cell's center [20], and its speed tends to be significantly higher close (within a few microns) to the leading edge of the cell [21]. Methods for evaluating the dynamics of individual protein species include fluorescence speckle microscopy (FSM), in which only a small portion of the molecules are tagged and followed, and image correlation spectroscopy, in which inhomogeneities in directional drift of fluorescence probes are detected. Both methods indicate that there is a spectrum of mobilities. The proteins that are most closely associated with integrins are nearly immobile, while those that are most closely associated with actin filaments are highly mobile [22–24]; intermediate behaviors are also seen. Recently, Gardel *et al* combined FSM with the estimation of forces from fiducial markers in a compliant polyacrylamide substrate coated with fibronectin [25]. Although their data are consistent with the earlier observed correlation between total forces on elastomeric posts and FA areas [9, 10], they found that the traction stress (force per area) exerted by epithelial cells depended most strongly on the local speed of the actin flow. The traction stress and flow speed are directly correlated at slow flow speeds and inversely correlated at fast flow speeds [25].

Here, we develop and analyze a simple microscopic model that links traction stresses and retrograde protein flow. In particular, it accounts for the biphasic relation between actin flow speed and traction stresses observed in epithelial cells [25]. The model is motivated by the observation that the motions of different molecules in FAs correlate to varying degrees with the motions of actin filaments [22], which suggests that layers of FA and cytoskeletal components can slip relative to each other. The traction stress is essentially a product of the force supported by a single such bond and the fraction of layer–layer molecular complexes formed. Molecular complexes must be displaced by the actin flow to stretch and transmit a force. Within this framework, we consider two behaviors for molecular complexes: slip bonds and catch bonds. For slip bonds, a load always favors dissociation, while for catch bonds there is a crossover from a small load regime in which tension favors association to a large load regime in which tension favors dissociation. The catch bond dynamics shift the peak of the overall biphasic trend toward higher actin flow speeds (such that the increasing and decreasing slopes are more similar) and, in turn, lead to better fits of the experimental data [25]. Our model further predicts that the stress–speed profile shifts as a whole to higher speeds for softer substrates and that the peak stress and the flow speed at this peak stress both increase for increased integrin–substrate affinity. The relationship with previous models [26–28] and cell movement is discussed.

2. The model

To develop a model that relates traction stresses to retrograde actin flow speeds, we represent the system by layers: (1) the actin cytoskeleton, which is taken to flow at a constant speed, (2) the FA, elements of which link to the surrounding layers, and (3) the substrate coated by ligands on the surface. We neglect many details of the system that are likely to modulate the behavior to focus on the essential physics; these details include signaling, aging of FAs, and the position and context of FAs within the cell. It will be interesting to extend the model as more information about FAs and their dynamics becomes available, but doing so is beyond the scope of the present study.

In the model, we imagine that actin flow can lead to breaking any of the many protein–protein interactions linking the substrate and the actin filament network, e.g. FA proteins binding directly to F-actin (α-actinin, vinculin, talin), protein interactions within FAs (paxillin and zyxin), and integrin binding to the ECM [22]. We model these dynamics by four sequential steps (figure 1(A)): (1) proteins encounter each other and form complexes; (2) complexes stretch elastically under the actin flow; (3) they break with extension-dependent kinetics; and (4) free proteins relax to their equilibrium conformation; the cycle then repeats. For clarity, we describe the model in terms of the engagement between integrin receptors and their ligands (e.g. fibronectin coating the substrate surface), but similar considerations are relevant to each such molecular interface.

Below, we describe the elementary mechanical and chemical interactions, particularly the mechanisms for breaking complexes of receptors and ligands. Master equations are then introduced to describe a population of such interactions and solved in the steady state. The behavior of the model is discussed under different assumptions and for varying choices of parameters. An extension of the model that includes the actin cytoskeleton layer enables connection with experiments that modulate the myosin activity and, in turn, the stress fiber density [25]. Experimentally testable predictions are made to further validate the model.

2.1. Flow-induced force

We represent receptors and their surface-associated ligands as linear springs with force constants k_r and k_l, respectively (figure 1(B)). We estimate k_l to be around 1 pN nm^{-1} by multiplying the literature value of Young's modulus of the substrate (1 kPa [25]) with the pertinent length scale (0.4 nm for fibronectin [29]). This value is consistent with previous measurements that are generally of the order of pN nm^{-1} [2, 30, 31]. To estimate k_r, we assume that the elastic

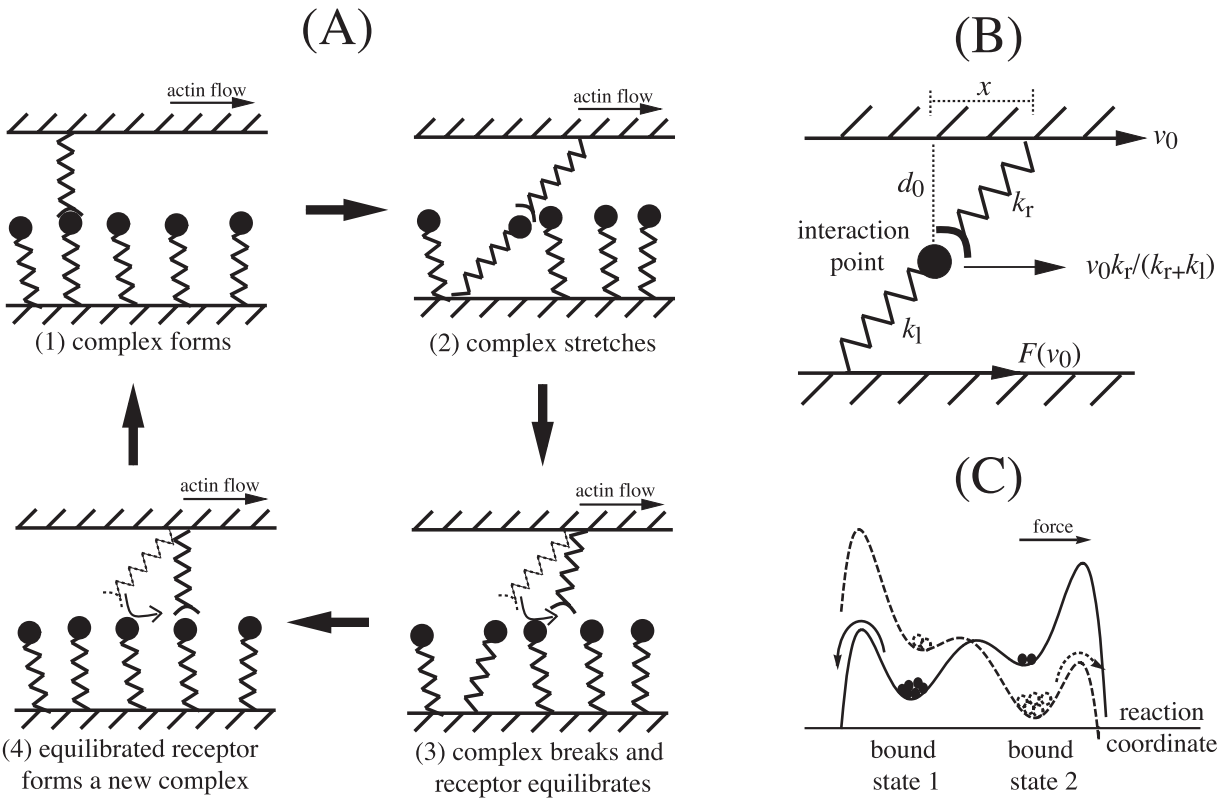

Figure 1. (A) The behaviors of integrin receptors and ligands under the actin flow: integrin receptors capture the ligands and form molecular complexes; complexes stretch elastically and break with extension-dependent kinetics; free receptors equilibrate to their natural length; the cycle repeats. (B) Schematic of the model. The top represents the focal adhesion moving with a speed v_0, and the bottom represents the ligand-coated substrate. The receptor and ligand stretch harmonically with force constants k_r and k_l, respectively. The interacting end of the receptor moves at a speed $v_0k_r/(k_r + k_l)$. Over a time interval, the movement of the top layer results in a horizontal extension x of the receptor and, in turn, a traction stress F on the substrate. The length of receptor is d_0 in the absence of stretch. (C) A mechanism for unbinding with two bound states and two pathways. The force raises (lowers) the barrier in the first (second) pathway and decreases the free energy difference of the second bound state to the first one. In the absence of force, the first bound state is preferred; as force increases, most molecules transit to the second bound state. Solid: free energy in the absence of force; dashed: free energy under the applied force.

properties of integrins are similar to those of the ligands on the substrate; then, the two spring constants are inversely related to their lengths according to Hooke's law for elastic materials. Fibronectin is a semiflexible polymer with a contour length of 60 nm [29] and the integrin head group has a length of 10–15 nm [32, 33], which indicates that receptors are several times stiffer than ligands.

As the upper layer in figure 1(B) moves, a bound complex stretches. As discussed immediately above, a molecular complex corresponds to two springs in series. Receptors and ligands stretch in inverse proportion to their spring constants (proportional to their lengths) when the force is uniform over the complex. Thus, the interacting point where a receptor and a ligand contact (figure 1(B)) will move at a speed $v_0k_r/(k_r + k_l)$ given one end of the complex moves at a speed v_0 and the other end is fixed. The collective effect is to exert a net flow $v_1 = v_0k_l/(k_r + k_l)$ on a bound receptor. Given the horizontal extension of an integrin x and the length of the integrin head group d_0, the force on the complex is $f(x) = k_r(\sqrt{x^2 + d_0^2} - d_0)$. The measured stress is the projection of the force onto the horizontal direction in figure 1(B).

2.2. Bond breaking

For the kinetics of bond breaking, we must assume a reasonable force-dependent free energy profile. Typically, the lifetime of a biological complex decreases when a sufficiently strong force pulls the bond. Such a bond is known as a 'slip bond'. Slip bonds occur because the force lowers the energy barrier between the bound and free states. A simple two-state (bound and unbound) model in which the lifetime decreases exponentially with force was introduced by Bell [34] and is employed frequently in the literature [35, 36]. More sophisticated versions were later introduced to account for the effects of mechanical forces on the rupture of molecular interactions [37, 38]. Because the flow speeds in the cell ($\sim$1 nm s^{-1} [25]) are slow in comparison to pulling speeds in typical single-molecule experiments on relevant systems ($\sim$1 μm s^{-1} [37]), the earlier phenomenological model [34] is adequate for our purposes.

In contrast, the lifetime of a 'catch bond' grows with applied force until a critical value, beyond which it shrinks [39–43]. To study this case, we consider two bound states with occupancies S_1 and S_2 and two pathways to the free state with unbinding rates k_1 and k_2 at zero force (figure 1(C)).

Transitions between the two bound states are allowed and assumed to be faster than unbinding, such that the ratio of the two bound states is equal to the exponential of the free energy difference, $\Phi = S_1/S_2 = \exp[(E_2 - E_1)/k_BT]$. Additionally, both pathways are assumed to be sensitive to force but in opposite ways. The force f raises (lowers) the barrier in the first (second) pathway by a factor $e^{\gamma_1 f}$ ($e^{\gamma_2 f}$) and also decreases the free energy difference of the second bound state to the first one by a factor $e^{\gamma_{12} f}$. Parameters γ_1, γ_2 and γ_{12} are determined by the positions of the bound states and the barriers in the reaction coordinate. In the absence of force, the first pathway is preferred; as force increases, the probability of breaking a bond decreases because of the higher barrier in the first pathway until most molecules transition to the second pathway. The equations for unbinding are $d(S_1 + S_2)/dt = -k_1 e^{-\gamma_1 f} S_1 - k_2 e^{\gamma_2 f} S_2$ and $S_1/S_2 = \Phi e^{-\gamma_{12} f}$; the effective unbinding rate is thus

$$k_u(f) = \frac{\Phi(k_1 e^{-\gamma_1 f}) + e^{\gamma_{12} f}(k_2 e^{\gamma_2 f})}{\Phi + e^{\gamma_{12} f}}. \quad (1)$$

The first term in the numerator accounts for the strengthening pathway and the second term accounts for the weakening pathway.

This mechanism simplifies to two existing catch bond models under extreme conditions. In the case that barrier heights are insensitive to the force ($\gamma_1, \gamma_2 = 0$), the effective rate becomes $k_u(f) = (\Phi k_1 + e^{\gamma_{12} f} k_2)/(\Phi + e^{\gamma_{12} f})$ as in [44]. Alternatively, if the relative likelihoods of the two bound states are held constant ($\gamma_{12} = 0$), the effective rate becomes

$$k_u(f) = k_u^1 e^{-\gamma_1 f} + k_u^2 e^{\gamma_2 f} \quad (2)$$

with $k_u^1 = k_1\Phi/(1 + \Phi)$ and $k_u^2 = k_2/(1 + \Phi)$. This form arises in a model that assumes a single bound state and two unbinding pathways [45, 46]. Moreover, if the first pathway is blocked, the model reduces to Bell's form of the slip bond and the effective rate becomes

$$k_u(f) = k_u^0 e^{\gamma f}. \quad (3)$$

In this paper, we explore three mechanisms for bond breaking as described by equations (1)–(3), and estimate the parameters in terms of the $\alpha_5\beta_1$ integrin–fibronectin complex. The unbinding rate is about 0.01 s^{-1}, and the transition state for unbinding is estimated to be at an extension of 1–5 Å [36]. Dividing temperature in energy units by this extension gives 10–50 pN of force required to break molecular interactions. Although catch bonds have been demonstrated for many receptor–ligand pairs, previous studies [36] did not observe this feature for integrins until recently [47, 48]. By measuring the force-dependent lifetimes of single bonds between a fibronectin fragment and an integrin $\alpha_5\beta_1$–F_c fusion protein or membrane $\alpha_5\beta_1$, the critical force for a transition from a catch bond to a slip bond is estimated to be around 30 pN and the lifetimes to be on the order of 10 s [47].

2.3. Bond formation

When a receptor dissociates, it can equilibrate to its natural conformation. A restoring force, $g(x)$, transforms the elastic energy stored during the extension of the molecular complex to a directional motion towards the natural conformation of the receptor; a friction force, $\lambda v_2(x)$, opposes this directional motion. These two forces balance in the over-damped limit and the velocity towards equilibrium $v_2(x)$ is $g(x)/\lambda$. The simplest form for the restoring force is a linear one: $g(x) = f(x) = k_r(\sqrt{x^2 + d_0^2} - d_0)$. For simplicity, we assume that only relaxed receptors form new complexes with ligands. In this case, the overall rate k_b is the intrinsic rate k_b^0 multiplied by a Gaussian factor, $k_b(x) = k_b^0 e^{-(x/x_0)^2}$.

To estimate the pseudo-first-order rate constant k_b^0, we follow Bell [34]. Namely, we assume receptors and ligands bind and unbind via a diffusive encounter complex (R · L):

$$R + L \underset{d_u}{\overset{d_b}{\rightleftharpoons}} R \cdot L \underset{r_u}{\overset{r_b}{\rightleftharpoons}} RL. \quad (4)$$

Then, within the quasi-steady-state approximation for the encounter complex, $K = k_u^0/k_b^0 = r_u d_u/(r_b d_b \rho_l)$, where ρ_l is the density of the ligand; $d_b/d_u = \pi R_{rl}^2$, where R_{rl} is the radius of the encounter complex. Taking $r_u/r_b = 0.01$ [36], $R_{rl} = 2$ nm [34, 49], and $\rho_l = 1000$ molecules μm^{-2} [50], we get $K = 1$. Because the lifetime of the complex is between 10 and 100 s [36, 47], we get $k_b^0 = 0.01$–0.1 s^{-1}.

2.4. Master equation

Because ligands are saturating in this system (the density of ligands $\rho_l = 1000$ molecules μm^{-2} is much larger than that of integrins $\rho_r = 2$–20 molecules μm^{-2} [25]), we focus on the dynamics of receptors in response to the actin flow v_0 in the upper layer. To this end, we assume that every receptor–ligand interaction behaves in an equivalent fashion and neglect variations in the kinetics that could arise from surface heterogeneity or context-dependent changes in the receptor activation state. We integrate the dynamics described above in master equations for the probabilities of observing bound and unbound receptors with horizontal extension x, denoted $P_b(x,t)$ and $P_u(x,t)$. The master equations are:

$$\frac{\partial P_b(x,t)}{\partial t} = -v_1 \frac{\partial P_b(x,t)}{\partial x} - k_u(f(x,t))P_b(x,t) + k_b(x)P_u(x,t) \quad (5)$$

$$\frac{\partial P_u(x,t)}{\partial t} = \frac{\partial [v_2^{\parallel}(x,t)P_u(x,t)]}{\partial x} + k_u(f(x,t))P_b(x,t) - k_b(x)P_u(x,t) \quad (6)$$

with $P_b(x,t)$ and $P_u(x,t)$ satisfying $\int_{-\infty}^{+\infty}[P_b(x,t) + P_u(x,t)]\,dx = 1$. The first term on the right-hand-side of equation (5) accounts for the shift in the upper layer relative to the lower layer. The form of this term is derived according to a conservation of probabilities in the absence of state changes. Using $v_1 = v_0 k_l/(k_l + k_r)$ instead of v_0 accounts for the net actin flow on receptors as shown in figure 1(B). The second and third terms, respectively, describe the unbinding and binding dynamics. The first term on the right-hand-side of equation (6) describes equilibration of receptors to their natural lengths under a horizontal velocity $v_2^{\parallel}(x,t)$. By assuming the restoring force to be a spring force, the velocity v_2 becomes

$k_r(\sqrt{x^2 + d_0^2} - d_0)/\lambda$. We neglect diffusion in the extension x because we found that it did not significantly affect the behavior of the model (not shown).

We are interested in the steady-state solution of the master equations (P_b^{ss} and P_u^{ss}; below, we designate other quantities in the steady state by 'ss' without further remarks; by the same token, projection from the diagonal direction along the spring to the direction of the traction stress parallel to the actin flow is denoted by '$\parallel$'), from which the traction stress on the ECM can be calculated as

$$F(v_0) = \rho_r \int_{-\infty}^{\infty} f^{\parallel}(x) P_b^{ss}(x, v_0)\, dx. \tag{7}$$

To this end, we rewrite the master equations:

$$\begin{aligned} &-v_1 \frac{\partial P_b^{ss}(x)}{\partial x} - k_u(f(x)) P_b^{ss}(x) + k_b(x) P_u^{ss}(x) = 0 \\ &\frac{\partial [v_2^{\parallel}(x) P_u^{ss}(x)]}{\partial x} + k_u(f(x)) P_b^{ss}(x) - k_b(x) P_u^{ss}(x) = 0. \end{aligned} \tag{8}$$

The actin-induced flow of bound receptors, v_1, and the equilibration of unbound receptors, $v_2^{\parallel}$, are in the same direction and tend to decrease the probability of a negative extension ($x < 0$). In the long-time limit, $P_b^{ss}(x < 0) = P_u^{ss}(x < 0) = 0$. Because the equations and the solutions are continuous at $x = 0$, the boundary conditions become $P_b^{ss}(0) = P_u^{ss}(0) = P_b^{ss}(\infty) = P_u^{ss}(\infty) = 0$, and the normalization condition becomes $\int_0^{\infty} [P_b^{ss}(x) + P_u^{ss}(x)]\, dx = 1$, if the parameters in equation (8) are bounded and nonzero. Summing the two equations in equation (8), it follows that $v_1 P_b^{ss}(x) - v_2^{\parallel}(x) P_u^{ss}(x) = 0$. Substituting this relation into equation (8) and integrating over x, we find that the probability distributions of bound and unbound receptors with horizontal displacement x are

$$\begin{aligned} &P_b^{ss}(x, v_0) \\ &= C(v_0) \exp\left[-\frac{1}{v_1} \int k_u(f(x))\, dx + \int \frac{k_b(x)}{v_2^{\parallel}(x)}\, dx \right] \\ &P_u^{ss}(x, v_0) \\ &= C(v_0) \exp\left[-\frac{1}{v_1} \int k_u(f(x))\, dx + \int \frac{k_b(x)}{v_2^{\parallel}(x)}\, dx \right] \frac{v_1}{v_2^{\parallel}(x)} \end{aligned} \tag{9}$$

where the constant $C(v_1)$ is determined by the normalization condition.

2.5. Results for the basic two-layer model

We solve the model in the steady state (equation (9)) for three molecular interaction scenarios: (1) slip bond (k_u as in equation (3)); (2) catch bond with a single bound state and two unbinding pathways (k_u as in equation (2)); (3) catch bond with two bound states and two unbinding pathways that allow interconversion (k_u as in equation (1)). The two catch bond scenarios differ with respect to the relative sizes of the ranges over which force enhances and reduces binding, as indicated by the lifetimes shown in figure 2(A). In all cases, the model

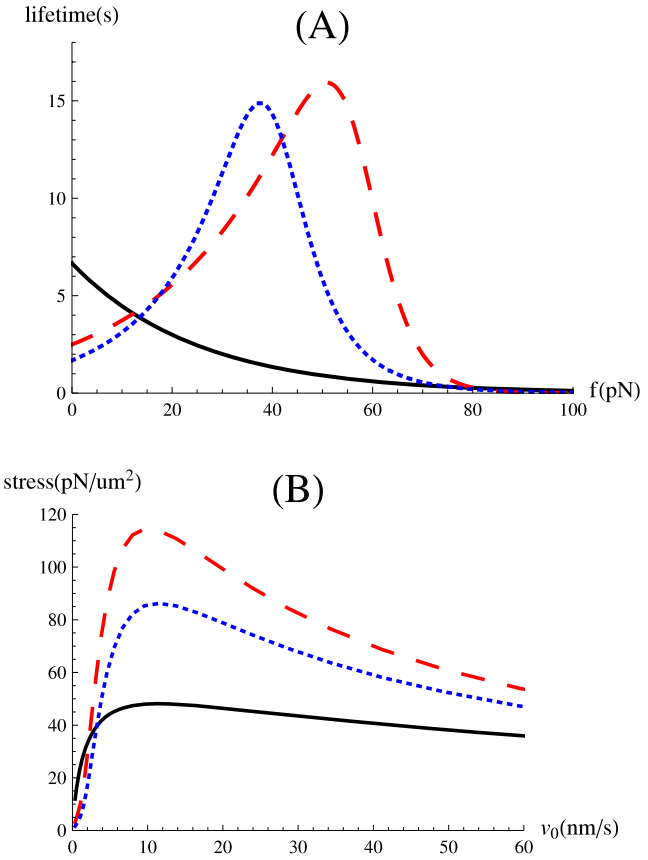

Figure 2. Different colors represent different types of bonds: solid, slip bond, $k_u = 0.15e^{0.04f}$; dashed, catch bond with one bound state and two unbinding pathways, $k_u = 0.4e^{-0.04f} + 4 \times 10^{-7}e^{0.2f}$; dotted, catch bond with two bound states and two unbinding pathways, $k_u = [100(0.6e^{-0.06f}) + e^{0.1f}(1.8 \times 10^{-3}e^{0.1f})]/(100 + e^{0.1f})$ (k_u in unit of s^{-1} and f in unit of pN). (A) Lifetimes of integrin receptor–ligand complexes under a force. (B) Dependence of traction stress on actin flow speed. Other parameters are given in choice of parameters, sensitivity and prediction.

exhibits the biphasic dependence of the traction stress on the actin flow speed, shown in figure 2(B). This can be understood as follows (figure 3). When there is no flow, the bound and unbound receptor populations equilibrate, and there is no net stretching of complexes and thus no force. At low flow rates, the traction stress increases as complexes deform. At high speeds, even though each bond to the substrate results in a larger traction stress, the number of bonds decreases with the speed.

For slip bonds, the traction stress increases linearly at low flow rates because of stretching, although the number of bonds decreases. However, for catch bonds receptors can be either above or below the critical force. The overall effect of intermediate flow rates can thus be either to increase or decrease the number of bound complexes (figure 3(A)). We find that the catch bond models enable better agreement with the experimental data. More specifically, we find that the greater the range over which the bond strengthens, the better the fit (figure 2). In interpreting this result, it is important to note that the catch bond representation in our model could serve to compensate for the neglect of force-

Table 1. Sensitivity of the results to parameter values. We scale dimensionless ratios of parameters that influence a specific feature of the biphasic dependence of traction stress on actin flow speed and present the results grouped by feature.

Feature affected	Dimensionless ratios scaled	Illustration
Slopes	$r_1 = k_u^1/k_u^2$, $r_2 = \gamma_1/\gamma_2$	Figure 2
Peak position (flow)	$\tilde{v} = (\gamma_2 k_e/k_u^2)v_0$ (with $k_e = k_r k_l/(k_r + k_l)$)	Figure 4(A)
Peak height (stress)	$K = k_u^2/k_b$, $\tilde{x}_0 = \gamma_2 k_r x_0$, $\tilde{\lambda} = (k_u^2/k_r)\lambda$, $\tilde{d}_0 = \gamma_2 k_r d_0$	Figure 4(B)

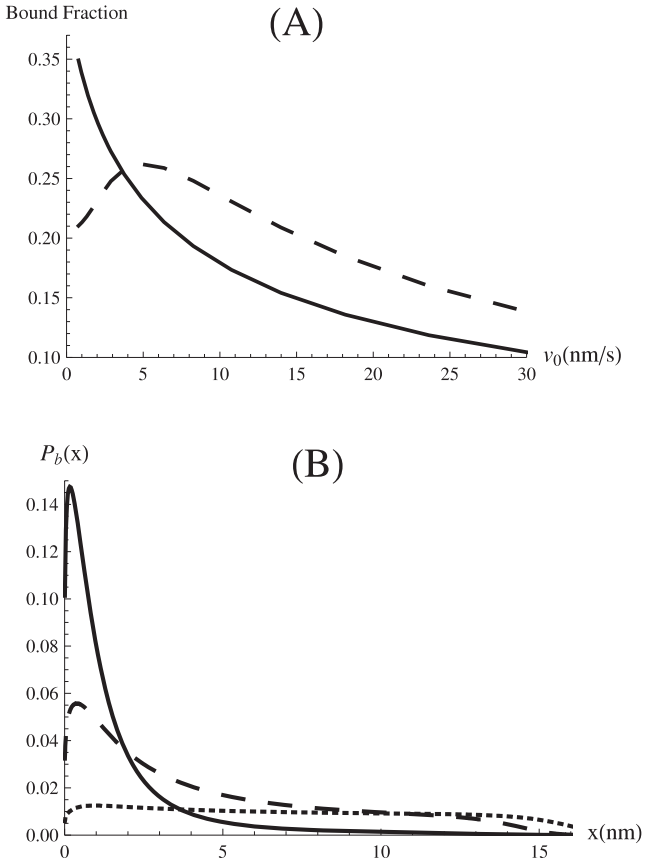

Figure 3. (A) The fraction of bound integrins as a function of actin flow speed: solid, slip bond (solid in figure 2); dashed, catch bond (dashed in figure 2). (B) The distribution of horizontal complex extension $P_b(x)$ under different actin flow speeds: v_0 equals to 2 (solid), 5 (dashed) and 25 (dotted) nm s^{-1}. Parameters are the same as the dashed curve in figure 2.

induced growth of focal adhesions and/or the coupling between the signaling and mechanical responses. Nevertheless, some form of strengthening with force appears to be important.

2.6. Choice of parameters, sensitivity, and predictions

The relevant parameter values are the effective properties of the composite materials at the interface (FAs in cells and the complete ligand-coated compliant substrate), which are unknown. To anchor the discussion, we choose values within reasonable ranges of data for integrins and their ligands; these values are then adjusted by hand to give traction stresses and flow speeds close to the actual measurements. In this section, we enumerate the parameters and their values unless otherwise indicated. Then, we explore the sensitivity of the results to these choices. The trends lead to experimentally testable predictions, which are detailed at the end.

The parameters related to the lifetime of a bond and how it is affected by the force include those in equations (1)–(3). They are chosen to make the average lifetimes of bonds between 10 and 100 s [36, 47] and the breaking force of the bond is about 100 pN (10–50 pN in [36], 50 pN in [47]). For catch bonds, the critical force is set to about 50 pN (30 pN in [47]). Other parameters are also acquired from the literature: the binding rate ($k_b = 0.1$ s^{-1}, as discussed in section 2.3), the friction coefficient ($\lambda = 10$ N s m^{-1} [26]), the length of an integrin ($d_0 = 15$ nm [32, 33]), and the density of receptors ($\rho_r = 20$ molecules μm^{-2} [51]). The spring constants for ligands and integrins are estimated to be $k_l = 1$ pN nm^{-1} and $k_r = 5$ pN nm^{-1} [31], respectively (see section 2.1). The parameter x_0 sets the range over which equilibrated integrins fluctuate, which is not known; we take it to be $x_0 = 1$ nm.

To study how parameters affect the model results, we assume the catch bond model in equation (2) and scale dimensionless ratios of parameters in equation (8). The biphasic behavior is found to be robust over the ranges examined, and the scaled parameters can be grouped into three categories based on how they affect other features in the stress–flow profile (table 1). The ratios r_1 and r_2 determine the extent of strengthening in the catch bond model, which affects the slopes as discussed in the previous section (figure 2). The only parameter to affect the peak position strongly is $\tilde{v}$: a higher value of $\gamma_2 k_e/k_u^2$ results in the same stress for a lower value of v_0 without changing the peak stress, which shifts the stress–speed profile leftward (figure 4(A)). The remainder of the parameters primarily impact the peak height, as follows:

- The ratio K is the intrinsic dissociation constant for the ligand–receptor complex. A larger K gives rise to weaker binding and thus less ability to support a force (figure 4(B)).
- The parameters $\tilde{x}_0$ and $\tilde{\lambda}$ affect the ability of integrins to rebind after a complex breaks. A larger $\tilde{x}_0$ or a smaller $\tilde{\lambda}$ increases the fraction of integrins that are able to bind with ligands and therefore the stress.
- The parameter $\tilde{d}_0$ determines the projection angle between directions of the spring force exerted on the molecular complex and the net force sensed on by the substrate. For a large $\tilde{d}_0$, little stress is sensed even when the diagonal force on bonds is sufficient to break them.

The parameters $\tilde{v}$ and K are experimentally accessible, and the trends described above for these parameters suggest means to validate the model experimentally. $\tilde{v}$ is accessible through the intrinsic unbinding rate for the receptor–ligand complex (k_u^1 and k_u^2) and the effective spring constant that

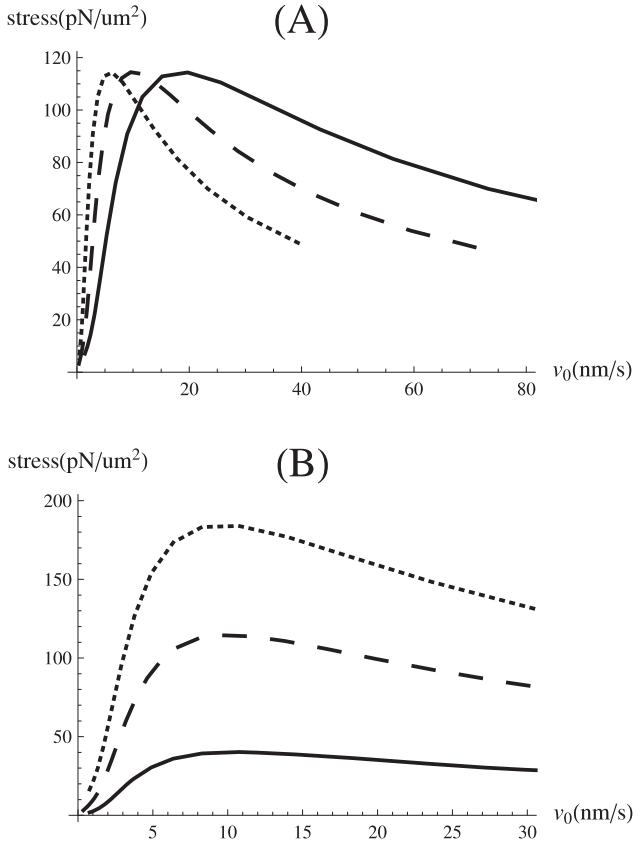

Figure 4. (A) Effect of varying the substrate stiffness, $k_l = 0.5$ (solid), 1 (dashed) and 2 (dotted) pN nm^{-1}. (B) Effect of varying the intrinsic binding rate, $k_b = 0.1$ (solid), 0.5 (dashed) and 2.5 (dotted) s^{-1}. Varying $\tilde{x}_0$, $\tilde{d}_0$ and $\tilde{\lambda}$ has similar effects as K, although trends may be opposite. Other parameters are the same as the dashed curve in figure 2.

characterizes the elastic properties of integrins and the ligand-coated surface at the microscopic scale ($k_e = k_r k_l/(k_r + k_l)$) (figure 4(A)). Alternatively, the traction stress can be modulated by changes in the concentration of ligands on the substrate and thus the ligand–receptor dissociation constant K. Favoring dissociation results in decreasing stress (figure 4(B)). In this regard, it is important to note that different ligands can recruit different integrin receptors; a change of receptor affects γ and k_r in addition to K, so care would be needed in interpreting experiments with different ligands. Indeed, this connection between receptors and ligands suggests that it will ultimately be of interest to experimentally map the 'phase' diagram for traction stresses as a function of different cell types and environments.

2.7. Variations in engagement of FAs and actin filaments

We now wish to extend the basic model to consider the coupling between the actin flow and the FA more explicitly. Doing so enables us to describe the qualitative effects of variations in the engagement of FAs and actin filaments resulting from modulation of myosin activity that regulates actin polymerization and the density of actin filaments

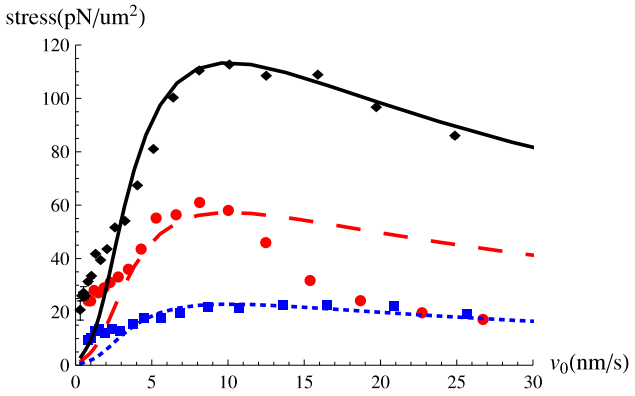

Figure 5. Traction stress for variations in stress fiber density. From top to bottom, $k_u^A/Ak_b^A = 0.01, 1, 4$. Lines are results from the model and points with error bars are experimental data (figure 4 of [25]). Other parameters are the same as the dashed curve in figure 2.

available for FAs [25]. To this end, we assume a quasi-equilibrium for the binding and unbinding of molecules in the FA to the actin filaments. Taking P_e to be the fraction of effectively engaged integrins, the flux balance condition gives $(1 - P_e)k_b^A A = k_u^A P_e$, where k_b^A and k_u^A are the rate constants for engaging and disengaging and A is the concentration of actin stress fibers. Solving for P_e in terms of A gives

$$P_e = \frac{1}{1 + k_u^A/(k_b^A A)}. \tag{10}$$

The measured stress is then the stress assuming all integrins are engaged (equation (7)) multiplied by the fraction that are engaged (P_e), which depends on the stress fiber density A and the dissociation constant $K^A = k_u^A/k_b^A$. As a result, variations in K^A or A shift the height of the stress–speed profile, without significantly influencing its peak position (figure 5). These trends are consistent with the effects of blebbistatin and a constitutively active form of Rho, which decrease and increase myosin activity and thus the stress fiber density A, respectively (see figure 4 of [25]).

2.8. Extension to multiple layers

In the basic model described above, we explicitly consider only two layers that interact through integrin receptors and their ligands. However, as mentioned in formulating the model, the actin flow can cause any of the many protein–protein interactions between the substrate and actin filament network to break [22]. We thus explore whether consideration of multiple layers could improve the fit with the experimentally measured traction stresses at intermediate stress fiber densities (the dashed curve in figure 5). Specifically, we consider a model comprising N layers ($N > 2$), and molecules in successive layers form and break bonds according to the same rules as integrin receptors and substrate ligands (figure 1). For simplicity, parameters for every layer are chosen to be the same. In other words, every layer has the same binding and unbinding kinetics, elastic properties, and molecular densities. Moreover, molecules in one layer are assumed to move at the

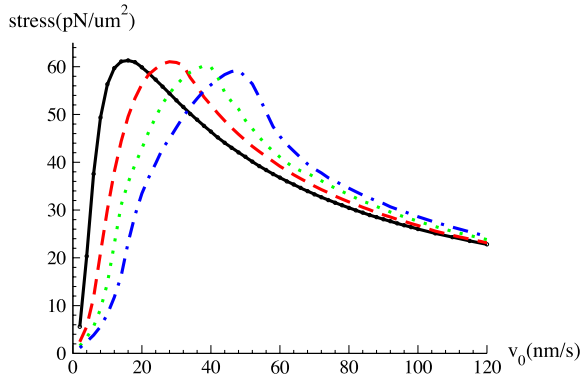

Figure 6. Traction stress for the multi-layer model. A thousand molecules are simulated in each layer. Parameters are the same as the red curve in figure 5. $N = 2$ (solid), 3 (dashed), 4 (dotted) and 5 (dashed-dotted).

same speed, denoted by v_i ($i = 0, 1, \ldots, N$); the top layer represents the actin filaments with speed v_0, and the bottom layer represents the substrate with speed $v_N = 0$ nm s^{-1}. The speed of a layer changes when the forces from the layers above and below it do not balance. The acceleration is the net force divided by the 'mass' of the layer, M. The mass determines the timescale in which the system converges to the steady state but not the steady state itself. The results shown are for $M = 1000$ pN s^2 nm^{-2}.

We treat the model numerically using a form of the Gillespie algorithm [52]. In the simulations, each layer is assumed to be well mixed, and the allowed reactions are the bonding and unbonding of receptors in layer i with ligands in layer $i + 1$ ($i = 0, 1, \ldots, N - 1$). The time interval between consecutive bonding or unbonding events (Δt) is stochastically determined by the Gillespie algorithm. Because $\Delta t < 0.02$ s in more than 96% of steps, it is small in comparison with the relaxation timescales of interest, and we treat the bond extensions and speeds of all layers as continuous variables for computational efficiency. Specifically, when a bond forms or breaks anywhere in the system, we integrate the continuous variables to first order for one step of length Δt.

Results are shown for $N = 2$–5 (figure 6). In all cases, each layer contains 1000 receptors. Ligands are assumed to be saturated as before and they affect the system through the binding rate k_b^0. Although ligand and receptor numbers are generally of the same order except the bottom layer, saturation is not a bad assumption given the fact that 25% of receptors at most form bonds between bottom layers $N - 1$ and N (the dashed curve in figure 3(A)) and fewer ligands in upper layers reduce the fraction. Other parameters are the same as the dashed curve in figure 5. Simulations last for 1500 s and reach steady states after 500 s. Traction stress is obtained by averaging from 1000 to 1500 s over 20 independent runs.

Interestingly, we observe two scenarios for the multiple-layer model (figure 7). At small retrograde actin flow speeds, the layers move at progressively slower speeds from top to bottom. At large speeds, layers move with either the top or the bottom layer, and there is a single interface between these groups. The sudden transition between these two dynamic

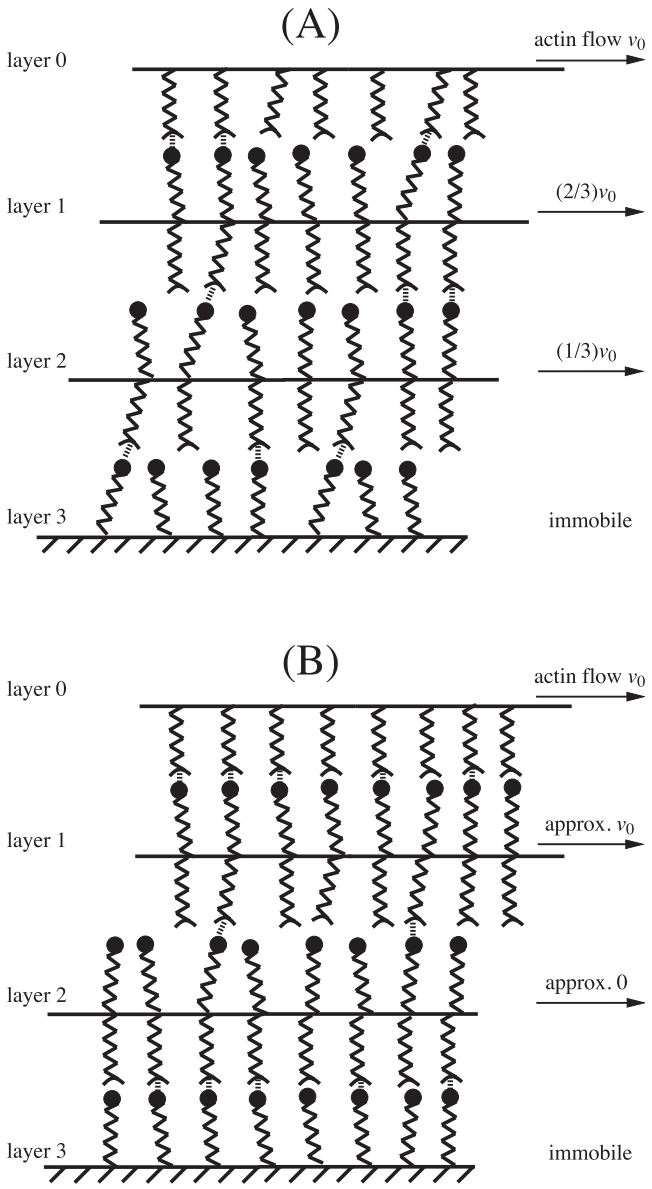

Figure 7. Scenarios observed for the multiple-layer model: (A) at small retrograde actin flow speeds, the layers move at progressively slower speeds from top to bottom; (B) at large speeds, layers move with either the top or bottom layer, and there is a single slipping interface between these groups. Dashed lines represent interacting receptors and ligands.

phases can be understood in terms of the stress–speed curve. Explicitly consider the case of $N = 3$. At a small v_0, layers moves roughly at v_0, $v_0/2$ and 0 from top to bottom. If the middle layer has a fluctuation resulting in an increase in speed, there is a decrease in the difference in speed relative to the top layer and an increase in the difference in speed relative to the bottom layer. There is less traction stress from the top and more from the bottom since the slope of the stress–speed curve is positive. The net effect is to work against the speed increase caused by the fluctuation, restoring the initial steady state. At higher speeds, the slope of the stress–speed curve becomes negative, which leads to an instability. If a fluctuation increases the speed of the middle layer, the traction from the top layer

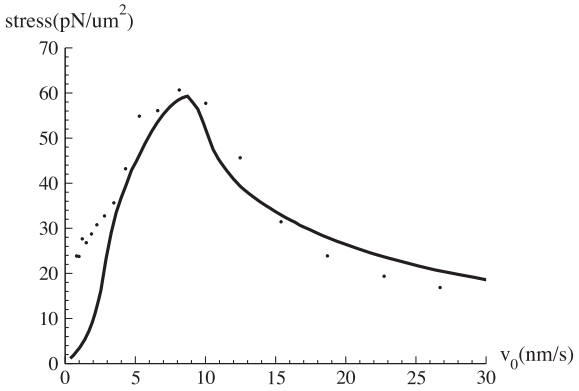

Figure 8. Comparison of numerical results for the multi-layer model (solid curve) with experimental data (dots; identical to the circular symbols in figure 5 [25]). Five layers are simulated with 1000 molecules in each layer. We choose the ligand stiffness in every layer k_l to be 5 pN nm^{-1}. Other parameters are the same as for the dashed curve in figure 5.

increases, but the traction from the bottom layer decreases. The net effect is to further accelerate the middle layer until the middle layer has the same speed as the actin layer.

Following the reasoning above, we can derive how the number of layers affects the traction and the critical actin flow speed that separates the two dynamic phases. We expect the critical speed of the N-layer case to be $(N-1)$-fold that of the basic (two-layer) model and the rough slope to be $1/(N-1)$ times that of the basic model below the critical speed. These estimates are supported by the numerical results (figure 6), although the transition between the two scenarios is blurred by the stochastic nature of the simulation.

The parameters used in the studies above are chosen to give the best fit of the basic model to the experimental data. However, by increasing the number of layers, we also shift the critical speed to larger values. We set $N = 5$ and adjust the ligand stiffness k_l to be 5 pN nm^{-1} to match the experimental data. As anticipated, the multi-layer model improves the fit to the experimental stress–speed profile (compare the dashed curve in figure 5 with figure 8). The left shoulder becomes softer because the actin flow is distributed among several layers, while the right shoulder becomes steeper due to the transition between two steady states. However, in the presence of blebbistatin (dotted curve in figure 5) or a constitutively active form of Rho (solid curve in figure 5), the basic model appears to perform better. The different N and k_l values required for the different conditions could reflect the fact that perturbing the myosin activity is likely to have many mechanistic consequences, but more molecular details need to be known before one can have confidence in this interpretation. Our purpose here is mainly to illustrate the qualitative trends for the stress–speed curve as one goes beyond the basic two-layer model.

3. Discussion

In the present study, we have shown that a microscopic model based on generic features of ligand–receptor complexes gives rise to a biphasic dependence of adhesion-derived traction stresses on the speed of retrograde flow of the actin filament network inside cells. When engaged, the cytoskeleton exerts a viscous drag on FAs due to constant binding and unbinding of receptor–ligand complexes. However, for sufficiently high flow speeds, protein rebinding rates become limiting and the cytoskeleton becomes progressively more disengaged. In other words, the model naturally gives rise to a clutch-like behavior.

The idea of a molecular clutch that regulates the mechanical coupling between the cytoskeleton and ECM adhesion points goes back at least two decades [53]. When the clutch is engaged, the retrograde actin flow generated by the myosin-derived contractile forces is transmitted via FAs to the substrate, resulting in a detectable traction stress. When the clutch is disengaged, the retrograde flow is fastest because the frictional force is absent and the FA/actin is in the slipping regime. In reality, there is likely to be a continuum of slipping interfaces between molecules rather than well-defined layers [22]. The value of the model is that it defines the consequences of a clutch-like mechanism precisely; it does not preclude the possibility that mechanical distortions of protein complexes and signaling [24] also contribute to the observed dynamics.

Because many features of our model are quite generic, they can be found in previous theoretical studies of FAs, in particular those of Bruinsma [26] and Chan *et al* [27]. Bruinsma [26] allowed for slipping between layers in order to account for the irreversible transition from a loosely engaged nascent complex to a tightly engaged mature FA at a critical force determined by the rigidity of the substrate. That model is mesoscopic in nature and treats the influence of the actin flow on the adhesion through a frictional drag. A key assumption in doing so is that the mechanical relaxation rather than the chemical steps are rate-limiting. This prevents the model from exhibiting the crossover in behaviors observed by Gardel *et al* [25], despite the fact that it is built on similar physics.

Chan *et al* also focused on the slipping between actin and the FAs, which are treated as part of a composite with the substrate. In other words, in their model molecular clutches are always engaged with substrate such that the extent of their movement is restricted. Chan *et al* examined the F-actin retrograde flow rates and the deformation of the FA–substrate composite (i.e., deflection of marker beads embedded in the substrate from their rest positions) depending on the substrate compliance. In the model, a stiff substrate gives rise to frictional slippage, where few clutches are engaged and the composite hardly moves. A soft substrate gives rise to a mode where many molecular clutches are engaged and the bulk goes through a periodic motion. The stress comes from the deformation of the composite during the periodic motion. Importantly, the model assumes a balance of the forces on the actin bundle, molecular clutches, and the substrate, and it constrains the forces and the speed of actin bundles to conform to a linear force–velocity relation of myosin motors: $v_{\text{filament}} = v_u(1 - F_{\text{substrate}}/F_{\text{stall}})$, where v_u is the unloading sliding velocity of myosin and F_{stall} is the stall force of myosin. A direct consequence of this relation is that the stress on the substrate is negatively related to the filament speed $F_{\text{substrate}} =$

$F_{\text{stall}}(1 - v_{\text{filament}}/v_{\text{u}})$, capturing only part of the biphasic behavior of interest here [25].

In the limit that integrins reach a quasi-equilibrium between their bound and unbound states, our model reduces to a mathematical form identical to that of a model of friction arising from bacterial propulsion [28]. In that study, the bacterial surface catalyzes actin polymerization and crosslinking to form a gel that moves away at a constant speed in the bacterial reference frame. A form equivalent to Bell's [34] (equation (3)) is used for the kinetics of the surface–gel interaction. The friction force plotted as a function of gel speed exhibits a crossover analogously to our model. A similar mathematical form has been employed in non-biological contexts as well, for example the friction arising from asperities on geological layers during earthquakes [54]. A negative correlation between the number of effective interacting elements and the interaction strength naturally gives rise to the crossover. The present study is important because it maps these physics to the specific experimental situation of interest [25], which leads to means for testing the applicability of the proposed mechanism. As illustrated by other models discussed above [26, 27], the connection to [28, 54] is by no means obvious. Moreover, our study provides new insights into the fundamental physics of molecular interfaces by comparing slip and catch bonds and in examining the dependence of the stress–speed profile on the number of molecular layers. Both these features significantly improve the ability to fit the experimental data.

It is of interest to consider how the biphasic dependence of traction stress on retrograde actin flow speed relates to lamellipodial protrusion and cell movement. In general, slower moving cells exhibit larger traction stresses [55] and faster retrograde flows of actin [56] and FA proteins [22, 57]. A biphasic relation between retrograde actin flow and adhesion was suggested previously based on the differing effects inhibiting myosin II activity with ML7 had on slow and fast moving keratocytes [56]. The protrusion rate decreased and the actin flow speed increased for the fast cells, while protrusion rate increased and the actin flow speed decreased for the slow cells. These observations are consistent with the fact that the higher stress curves envelop the lower stress curves in figure 5, such that adhesions on either side of the peak would 'collapse' inward in shifting from the higher to the lower curve. However, cell movement is very complex, and many other factors are likely to contribute to these dynamics. As a first step toward solidifying the link between retrograde flow, traction stresses, and protrusion, it will be of interest in the future to combine local, microscopic models like that considered here with mesoscopic models capable of treating contractility and movement at the level of whole cells [58–60].

Acknowledgments

We wish to thank Margaret Gardel, Yvonne Aratyn, Shannon Stewman, and Fred Mackintosh for helpful discussions. This work was supported by the National Science Foundation Materials Research Science and Engineering Center at the University of Chicago (grant no. NSF-DMR-0820054) and a MURI grant from the Army Research Office.

References

[1] Burridge K and Chrzanowska-Wodnicka M 1996 Focal adhesions, contractility, and signaling *Annu. Rev. Cell Dev. Biol.* **12** 463–519
[2] Geiger B, Bershadsky A, Pankov R and Yamada K M 2001 Transmembrane extracellular matrix-cytoskeleton crosstalk *Nat. Rev. Mol. Cell Biol.* **2** 793–805
[3] Bershadsky A, Kozlov M and Geiger B 2006 Adhesion-mediated mechanosensitivity: a time to experiment, and a time to theorize *Curr. Opin. Cell Biol.* **18** 472–81
[4] Harris A K, Wild P and Stopak D 1980 Silicone rubber substrata: a new wrinkle in the study of cell locomotion *Science* **208** 177–9
[5] Lee J, Leonard M, Oliver T, Ishihara A and Jacobson K 1994 Traction forces generated by locomoting keratocytes *J. Cell Biol.* **127** 1957–64
[6] Oliver T, Jacobson K and Dembo M 1995 Traction forces in locomoting cells *Cell Motil. Cytoskelton* **31** 225–40
[7] Dembo M and Wang Y-L 1999 Stresses at the cell-to-substrate interface during locomotion of fibroblasts *Biophys. J.* **76** 2307–16
[8] Galbraith C G and Sheetz M P 1997 A micromachined device provides a new bend on fibroblast traction forces *Proc. Natl Acad. Sci. USA* **94** 9114–8
[9] Balaban N Q, Schwarz U S, Riveline D, Goichberg P, Tzur G, Sabanay I, Mahalu D, Safran S, Bershadsky A, Addadi L and Geiger B 2001 Force and focal adhesion assembly: a close relationship studied using elastic micropatterned substrates *Nat. Cell Biol.* **3** 466–72
[10] Tan J L, Tien J, Pirone D M, Gray D S, Bhadriraju K and Chen C S 2003 Cells lying on a bed of microneedles: an approach to isolate mechanical force *Proc. Natl Acad. Sci. USA* **100** 1484–9
[11] Riveline D, Zamir E, Balaban N Q, Schwarz U S, Ishizaki T, Narumiya S, Kam Z, Geiger B and Bershadsky A D 2001 Focal contacts as mechanosensors: externally applied local mechanical force induces growth of focal contacts by an mDia1-dependent and ROCK-independent mechanism *J. Cell Biol.* **153** 1175–86
[12] Choquet D, Felsenfeld D P and Sheetz M P 1997 Extracellular matrix rigidity causes strengthening of integrin-cytoskeleton linkages *Cell* **88** 39–48
[13] Katz B-Z, Zamir E, Bershadsky A, Kam Z, Yamada K M and Geiger B 2000 Physical state of the extracellular matrix regulates the structure and molecular composition of cell–matrix adhesions *Mol. Biol. Cell* **11** 1047–60
[14] Nicolas A, Geiger B and Safran S A 2004 Cell mechanosensitivity controls the anisotropy of focal adhesions *Proc. Natl Acad. Sci. USA* **101** 12520–5
[15] Shemesh T, Geiger B, Bershadsky A D and Kozlov M M 2005 Focal adhesions as mechanosensors: a physical mechanism *Proc. Natl Acad. Sci. USA* **102** 12383–8
[16] Nicolas A and Safran S A 2006 Limitation of cell adhesion by the elasticity of the extracellular matrix *Biophys. J.* **91** 61–73
[17] Besser A and Safran S A 2006 Force-induced adsorption and anisotropic growth of focal adhesions *Biophys. J.* **90** 3469–84
[18] Aroush D R and Wagner H D 2006 Shear–stress profile along a cell focal adhesion *Adv. Mater.* **18** 1537–40
[19] Gov N S 2006 Modeling the size distribution of focal adhesions *Biophys. J.* **91** 2844–7
[20] Wang Y L 1985 Exchange of actin subunits at the leading edge of living fibroblasts: possible role of treadmilling *J. Cell Biol.* **101** 597–602
[21] Ponti A, Machacek M, Gupton S L, Waterman-Storer C M and Danuser G 2004 Two distinct actin networks drive the protrusion of migrating cells *Science* **305** 1782–6

[22] Hu K, Ji L, Applegate K T, Danuser G and Waterman-Storer C M 2007 Differential transmission of actin motion within focal adhesions *Science* **315** 111–5
[23] Brown C M, Herbert B, Kolin D L, Zareno J, Whitmore L, Horwitz A R and Wiseman P W 2006 Probing the integrin-actin linkage using high-resolution protein velocity mapping *J. Cell Sci.* **119** 5204–14
[24] Wang Y-L 2007 Flux at focal adhesions: slippage clutch, mechanical gauge, or signal depot *Sci. STKE* **2007** pe10
[25] Gardel M L, Sabass B, Ji L, Danuser G, Schwarz U and Waterman C M 2008 Traction stress in focal adhesions correlates biphasically with actin retrograde flow speed *J. Cell Biol.* **183** 999–1005
[26] Bruinsma R 2005 Theory of force regulation by nascent adhesion sites *Biophys. J.* **89** 87–94
[27] Chan C E and Odde D J 2008 Traction dynamics of filopodia on compliant substrates *Science* **322** 1687
[28] Gerbal F, Chaikin P, Rabin Y and Prost J 2000 An elastic analysis of listeria monocytogenes propulsion *Biophys. J.* **79** 2259–75
[29] Erdmann T and Schwarz U S 2006 Bistability of cell–matrix adhesions resulting from nonlinear receptor–ligand dynamics *Biophys. J* **91** L60–2
[30] Taubenberger A, Cisneros D A, Friedrichs J, Puech P-H, Muller D J and Franz C M 2007 Revealing early steps of $\alpha_2\beta_1$ integrin-mediated adhesion to collagen type I by using single-cell force spectroscopy *Mol. Biol. Cell* **18** 1634–44
[31] Fisher T E, Oberhauser A F, Carrion-Vazquez M, Marszalek P E and Fernandez J M 1999 The study of protein mechanics with the atomic force microscope *Trends Biochem. Sci.* **24** 379–84
[32] Hynes R O 1992 Integrins-versatility, modulation, and signaling in cell-adhesion *Cell* **69** 11–25
[33] Zamir E and Geiger B 2001 Molecular complexity and dynamics of cell–matrix adhesions *J. Cell Sci.* **114** 3583–90
[34] Bell G I 1978 Models for the specific adhesion of cells to cells *Science* **200** 618–27
[35] Evans E A and Calderwood D A 2007 Forces and bond dynamics in cell adhesion *Science* **316** 1148–53
[36] Li F, Redick S D, Erickson H P and Moy V T 2003 Force measurements of the $\alpha_5\beta_1$ integrin–fibronectin interaction *Biophys. J.* **84** 1252–62
[37] Hummer G and Szabo A 2003 Kinetics from nonequilibrium single-molecule pulling experiments *Biophys. J.* **85** 5–15
[38] Friddle R W 2008 Unified model of dynamic forced barrier crossing in single molecules *Phys. Rev. Lett.* **100** 138302
[39] Marshall B T, Long M, Piper J W, Yago T, McEver R P and Zhu C 2003 Direct observation of catch bonds involving cell-adhesion molecules *Nature* **423** 190–3
[40] Guo B and Guilford W H 2006 Mechanics of actomyosin bonds in different nucleotide states are tuned to muscle contraction *Proc. Natl Acad. Sci. USA* **103** 9844–9
[41] Sarangapani K K, Yago T, Klopocki A G, Laurence M B, Fieger C B, Rosen S D, McEver R P and Zhu C 2004 Low force decelerates L-selectin dissociation from P-selectin glycoprotein ligand-1 and endoglycan *J. Biol. Chem.* **279** 2291–8
[42] Yakovenko O, Sharma S, Forero M, Tchesnokova V, Aprikian P, Kidd B, Mach A, Vogel V, Sokurenko E and Thomas W E 2008 Fimh forms catch bonds that are enhanced by mechnical force due to allosteric regulation *J. Biol. Chem.* **283** 11596–605
[43] Yago T, Lou J, Wu T, Yang J, Miner J J, Coburn L, Lopez J A, Cruz M A, Dong J F, McIntire L V, McEver R P and Zhu C 2008 Platelet glycoprotein Ibα forms catch bonds with human WT vWF but not with type 2B von Willebrand disease vWF *J. Clin. Invest.* **118** 3195–207
[44] Evans E, Leung A, Heinrich V and Zhu C 2004 Mechanical switching and coupling between two dissociation pathways in a p-selectin adhesion bond *Proc. Natl Acad. Sci. USA* **101** 11281–6
[45] Perezerzev Y V, Prezhdo O V, Forero M, Sokurenko E V and Thomas W E 2005 The two-pathway model for the catch-slip transition in biological adhesion *Biophys. J.* **89** 1446–54
[46] Perezerzev Y V, Prezhdo O V, Thomas W E and Sokurenko E V 2005 Distinctive features of the biological catch bond in the jump-ramp force regime predicted by the two-pathway model *Phys. Rev.* E **72** 010903
[47] Kong F, Garcia A J, Mould A P, Humphries M J and Zhu C 2009 Demonstration of catch bonds between an integrin and its ligand *J. Cell Biol.* **185** 1275–84
[48] Puklin-Faucher E and Vogel V 2009 Integrin activation dynamics between the RGD-binding site and the headpiece hinge *J. Biol. Chem.* **284** 36557–68
[49] Lauffenburger D A and Linderman J J 1993 *Receptors: Models for Binding, Trafficking, and Signaling* (Oxford: Oxford University Press)
[50] Thoumine O, Kocian P and Kottelat A 2000 Short-term binding of fibroblasts to fibronectin: optical tweezers experiments and probabilistic analysis *Eur. Biophys. J.* **29** 398–408
[51] Bell G I, Dembo M and Bongrand P 1984 Cell adhesion-competition between nonspecific repulsion and specific bonding *Biophys. J.* **45** 1051–64
[52] Gillespie D T 1977 Exact stochastic simulation of coupled chemical reactions *J. Phys. Chem.* **81** 2340–61
[53] Mitchison T and Kirschner M 1988 Cytoskeletal dynamics and nerve growth *Neuron* **1** 761–72
[54] Braun O M and Peyrard M 2008 Modeling friction on a mesoscale: Master equation for the earthquakelike model *Phys. Rev. Lett.* **100** 125501
[55] Harris A K, Stopak D and Wild P 1981 Fibroblast traction as a mechanism for collagen morphogenesis *Nature* **290** 249–51
[56] Jurado C, Haserick J R and Lee J 2005 Slipping or gripping? Fluorescent speckle microscopy in fish keratocytes reveals two different mechanisms for generating a retrograde flow of actin *Mol. Biol. Cell* **16** 507–18
[57] Guo W-H and Wang Y-L 2007 Retrograde fluxes of focal adhesion proteins in response to cell migration and mechanical signals *Mol. Biol. Cell* **18** 4519–27
[58] Kruse K, Joanny J F, Julicher F and Prost J 2006 Contractility and retrograde flow in lamellipodium motion *Phys. Biol.* **3** 130–7
[59] Deshpande V S, McMeeking R M and Evans A G 2006 A bio-chemo-mechanical model for cell contractility *Proc. Natl Acad. Sci. USA* **103** 14015–20
[60] Yang T and Zaman M H 2007 Regulation of cell adhesion free energy by external sliding forces *Exp. Mech.* **49** 57–63